J Porous Mater (2016) 23:1155–1162
DOI 10.1007/s10934-016-0173-4

ORIGINAL PAPER

CO_2 adsorption at high pressures in MCM-41 and derived alkali-containing samples: the role of the textural properties and chemical affinity

Margarita J. Ramírez-Moreno[1] · Issis C. Romero-Ibarra[2] · Mateo González-de Gortari[1] · Ángeles Hernández-Pérez[3] · Heriberto Pfeiffer[1]

Published online: 5 April 2016

Abstract The adsorption properties of N_2 and CO_2 of MCM-41 and derived alkali-containing samples were analyzed over a wide range of pressures (up to ~4500 kPa) and temperatures (between 30 and 300 °C). The high-pressure and high-temperature experiments were carried out on pure MCM-41 and K- and Na-impregnated derived samples. It was analyzed the influence of pressure and temperature on the CO_2 capture capacity on pure and impregnated samples. The adsorption performance was correlated to the structure and textural properties of the materials using X-ray diffraction and N_2 adsorption–desorption measurements. The addition of an alkaline element changes the textural properties of the material increasing the pore size, which positively affected the CO_2 adsorption capacity of these materials at high pressure. In addition, the isosteric heats of adsorption gave information about the chemical affinity between the impregnated materials and CO_2. The CO_2 adsorption at ~ 4500 kPa for the samples with 5 wt% Na at 100 and 200 °C were 77.98 and 9.79 mmol g^{-1}, respectively, while the pure MCM-41 adsorbs only 8.92 mmol g^{-1}.

Keywords Mesoporous molecular sieve · MCM-41 · High pressure · CO_2 sorption

1 Introduction

Carbon dioxide (CO_2) capture, storage and utilization technologies are useful for reducing greenhouse gases contributing to global warming [1–3]. Recent studies have been focused on the separation of CO_2 from flue gases via several methods, such as absorption by liquids, adsorption onto porous solids and membrane purification. Adsorption is considered to be a competitive and viable method for CO_2 removal in comparison to other technologies [3]. The separation and purification of gas mixtures have become a major operation in the chemical and petrochemical industries [3, 4]. Various adsorbents, such as activated carbons, pillared clays, metal oxides, amine-based adsorbents, metal organic frameworks (MOF) and molecular sieves (zeolites and MCM-41) have been investigated [1–14]. Silica-based mesoporous molecular sieves are capable of adsorbing molecules, exchanging cations and catalyzing numerous industrially important reactions [13, 15]. Mesoporous materials have attracted considerable attention due to their gas adsorption capability, which is associated with their unique properties, including their periodic ordered mesoporous structure, large pore size, narrow pore size distribution and large surface area. Thus, these materials have potential applications in many fields of applied chemistry, such as catalysis, adsorption, separation and host-guest chemistry [15–18]. In particular, MCM-41 molecular

✉ Heriberto Pfeiffer
pfeiffer@iim.unam.mx

[1] Instituto de Investigaciones en Materiales, Universidad Nacional Autónoma de México, Circuito exterior s/n, Ciudad Universitaria, Del. Coyoacán, CP 04510 Ciudad de México, Mexico

[2] Unidad Profesional Interdisciplinaria en Ingeniería y Tecnologías Avanzadas, Instituto Politécnico Nacional, Av. IPN No. 2580, Col. Barrio la Laguna Ticomán, Gustavo A. Madero, CP 07340 Ciudad de México, Mexico

[3] Departamento de Ingeniería en Metalurgia y de Materiales, Escuela Superior de Ingeniería Química e Industrias Extractivas, Instituto Politécnico Nacional, UPALM, Av. Instituto Politécnico Nacional s/n, CP 07738 Ciudad de México, Mexico

sieves are promising materials for diverse applications and fundamental studies [2, 6–12, 15–17].

In recent years, high-pressure adsorption has been applied in industrial adsorption processes. Therefore, it is important to identify the best adsorbents and the optimal pressure conditions that lead to high storage capacities. Experimental studies are also necessary to characterize the performances of adsorption heat pumps, thermo transformers, refrigerating machines and post-combustion processes [6]. High-pressure adsorption measurements are of general interest in connection with different emerging technologies such as natural gas and hydrogen storage or high-pressure gas separation; the development of these emerging technologies requires basic adsorption data over a wide range of experimental conditions, such as temperatures above room temperature and/or high pressures [2, 18]. Recently, Zhuo et al. [19] reported a molecular simulation of the adsorption of CO_2, N_2 on MCM-41. Belmabkhout et al. [3] studied the sorption of pure CO_2; they showed that MCM-41 molecular sieves exhibit promising CO_2 adsorption properties at ambient temperature and high pressure in terms of the CO_2 uptake in dry conditions, adsorption kinetics and regeneration. Based on these findings, it was inferred that MCM-41 molecular sieve is a promising physical adsorbent for CO_2 capture at high pressure, showing a viable combination of CO_2 working adsorption capacity, adsorption rate and regeneration. Although CO_2 adsorption studies have been performed, the mesoporous materials have not been extensively studied at high pressures.

Because of its practical relevance, in this work, the N_2 and CO_2 adsorptions at high pressures on pristine and derived alkali-containing samples were investigated over a wide range of pressures (up to 4500 kPa) and temperatures (between 30 and 300 °C). The influence of high pressures on the structures of the pristine MCM-41 and impregnated (Na- and K-) samples was examined using X-ray diffraction, infrared spectroscopy and N_2 adsorption measurements. Also, the isosteric heats of adsorption were calculated to elucidate the chemical affinity between the alkali-containing materials and CO_2.

2 Experimental section

Commercial MCM-41 (~3 % aluminum content and a density equal to 2.6 g cm^{-3}) was purchased from Sigma Aldrich (CAS # 643653) and then derived alkali-containing samples were prepared as follows. Appropriate quantities of NaOH and KOH were dissolved into distilled water to prepare two 1 M solutions. Different quantities of each solution were added drop wise to MCM-41 to obtain 5 wt% Na- and 5 and 10 wt% K-derived alkali-containing samples. After that, all the samples were dried at 80 °C for 8 h to obtain powder materials. The materials were labeled as 5Na, 5 K and 10 K for the sodium- and potassium-derived alkali-containing samples.

Sorption isotherms at high pressure were recorded using a Belsorp-HP volumetric instrument from Bel-Japan Inc. The experiments were performed at specific temperatures (30, 70, 100, 200 and 300 °C), while the pressure was increased up to 4500 kPa. It is important to mention that only the pure MCM-41 sample was used for the N_2 high-pressure adsorption analysis at the different temperatures.

MCM-41 is sensitive to the presence of moisture, showing high affinity to humidity at high relative pressures of water vapor [3]. Thus, the materials were dried at 300 °C for 4 h before the N_2 or CO_2 sorption tests. In all cases, a similar quantity of sample was used in each measurement. N_2 and He gases were purchased from PRAXAIR Mexico with purities equal to 99.998 and 99.995 vol%, respectively, and CO_2 was provided by INFRA Mexico with a purity of 99.8 vol%.

Pure MCM-41 and derived alkali-containing samples were characterized by X-ray diffraction (XRD) using a D5000 diffractometer from Siemens with a Co $K\alpha_1$ radiation and a D8 Bruker X-ray diffractometer coupled to a Cu $K\alpha_1$ anode X-ray tube to determine the mesoporous ordering and amorphous structure, respectively.

Additionally, the textural properties of the samples were determined by N_2 adsorption–desorption measurements using a Minisorp II from Bel-Japan at 77 K employing the BET method [20, 21]. The samples were pretreated at room temperature under high vacuum for 24 h. The pure and derived alkali-containing samples were analyzed before and after the high pressure CO_2 experiments. Also, the addition and content of the alkaline elements was confirmed by Energy Dispersive X-ray Spectroscopy (EDS) analysis in a JEOL JMS-7600F (data not shown).

3 Results and discussion

The structure and microstructure of the pure MCM-41 commercial sample was characterized by XRD and N_2 adsorption–desorption measurements. Figure 1 shows XRD patterns of the initial mesostructured aluminosilicate sample at different 2θ ranges. The XRD pattern obtained between 10° and 75° in 2θ (Fig. 1a) shows a single wide peak between 15° and 40°, characteristics of the global amorphous structure of the material. In contrast, the low angle (2–8°) XRD analysis (Fig. 1b) shows the typical diffraction pattern associated with the mesoporous ordering of the MCM-41, where the (100), (110), (200) and (210) reflections are evidenced [6, 15]. These peaks are

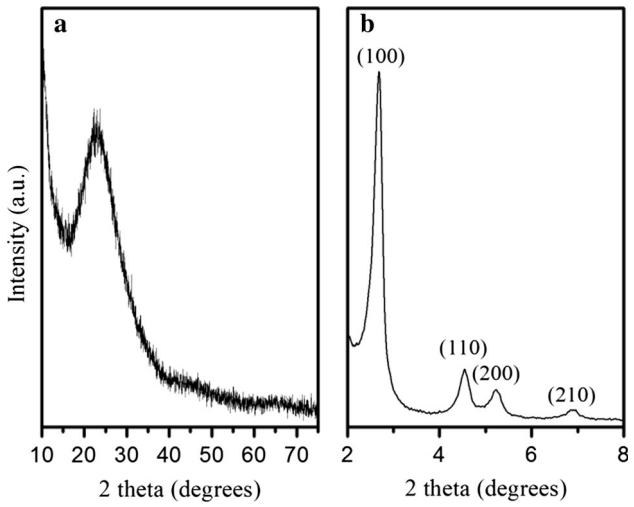

Fig. 1 Standard (**a**) and low angle (**b**) XRD patterns of the commercial pure MCM-41

associated with the ordered hexagonal array of parallel silica tubes and can be indexed assuming a hexagonal unit cell.

The textural properties of the sample were determined using N_2 adsorption–desorption measurements. Figure 2 shows the N_2 adsorption–desorption isotherm as well as the BET surface area, mean diameter (ϕ_p) and total pore volume of the mesopores. The N_2 adsorption–desorption isotherm corresponds to a type IV isotherm, which exhibits an H4-type hysteresis loop according to the IUPAC classification, this adsorption–desorption-behavior is characteristic of compounds with a nanopore size distribution in the micro and mesoporous range [20–22]. Additionally, the microstructural data were obtained using the BET method, where the pristine MCM-41 sample has a surface area of 984.3 m^2/g, a total pore volume of 1.0 cm^3/g and a pore diameter of 4.39 nm, (236.6 m^2/g and 1.10 nm correspond a surface area and a pore diameter in the microporosity range).

After the MCM-41 characterization, different fractions of the sample were impregnated with 5 wt% of Na or K. Figure 3 shows the XRD patterns of the derived alkali-containing samples, the amorphous phase was not modified. However, the microstructural characteristics completely changed. Figure 4 shows the N_2 adsorption–desorption isotherms obtained for the different derived alkali-containing samples. A third sample containing 10 wt% of K (10 K) was prepared and characterized for comparison purposes. Despite the 10 K sample shows a similar XRD pattern than those of 5Na and 5 K (data not shown), this sample showed similar textural properties to 5Na.

The N_2 adsorption–desorption isotherms of the derived alkali-containing samples presented type II-b isotherms with narrow H3-type hysteresis loops [20, 21], this desorption behavior is due to the low degree of pore curvature and the non-rigidity of the adsorbent structure [19, 23]. Although the surface area and the total pore volume decreased depending on the alkaline element amount added, the pore diameter tended to increase as (see Table 1). The addition of Na and K (5 wt%) resulted in a decrease of the surface area from 984.3 m^2/g (initial sample) to 100.0 and 296.9 m^2/g, respectively. However, the pore diameter increased to 8.8 and 11.7 nm in the 5 K and 5Na samples (Fig. 5), respectively, from the 4.3 nm observed in the pure MCM-41. In the 10 K sample, the final surface area decreased to 92.7 m^2/g and the pore diameter was 10.7 nm.

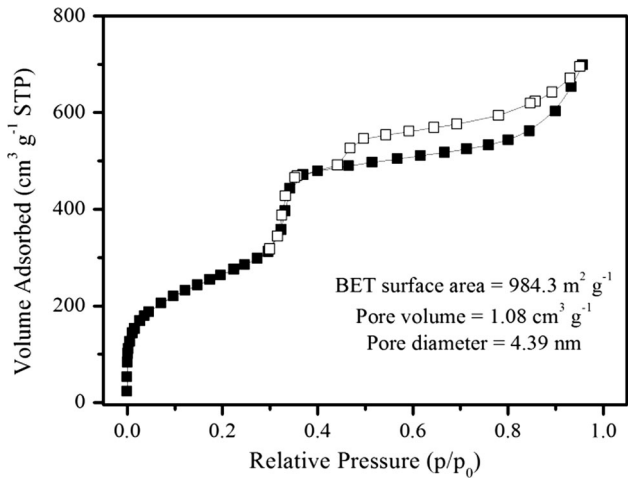

Fig. 2 N_2 adsorption–desorption isotherm of the MCM-41 sample. Microstructural characteristics were determined using the BET (surface area) model

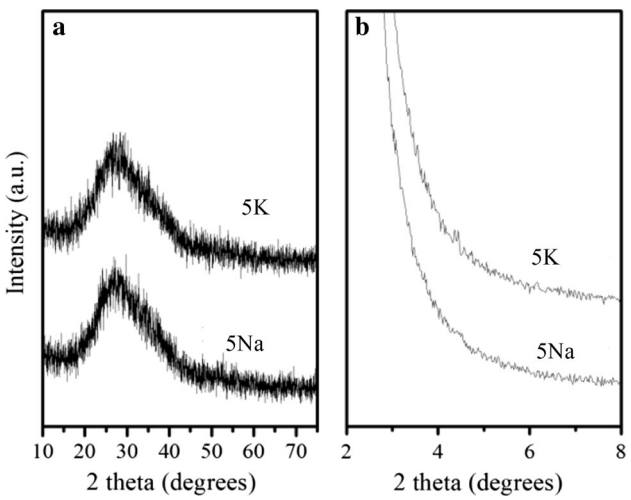

Fig. 3 Standard (**a**) and low angle (**b**) XRD patterns of 5-Na and 5-K derived alkali-containing samples

Summarizing the microstructural characterization results, the mesoporous order was destroyed by the addition of the alkaline elements. The total pore volume decreased with the addition of K and Na, along with the surface areas, but the pore diameters increased. It seems that K and Na modified the MCM-41 mesoporous walls, destroying the porous ordering, decreasing the area and pore volume. Nevertheless, the alkaline chemical attack may have dissolved or destroyed the porous walls of two or three neighboring pores, producing a new pore with a larger diameter. Additionally, the microstructure's degradation seems to show the following trend; Na > K (Table 1).

After the samples characterization, pristine MCM-41 and derived alkali-containing samples were tested in the high pressure capture process at different temperatures. Initially, the thermal and pressure stability of the MCM-41 sample was evaluated using N_2 as an adsorbing gas. Figure 6 shows the N_2 adsorption isotherms performed at different temperatures (between 30 and 200 °C). At 30 °C, the MCM-41 sample adsorbed up to 34.06 cm^3/g (1.52 mmol/g) of N_2 at ~5600 kPa. At 70 and 100 °C, the curves displayed the same behavior, and the N_2 adsorption maxima were 31.73 and 27.12 cm^3/g (1.42 and 1.21 mmol/g) respectively. However, when the temperature was increased to 200 °C an abrupt change occurred, and the maximum N_2 amount captured was ~12.05 cm^3/g

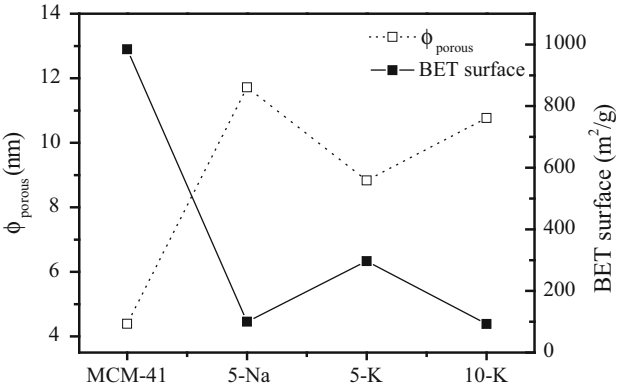

Fig. 5 Comparative surface area and porous diameter curves of the MCM-41 and derived alkali-containing samples

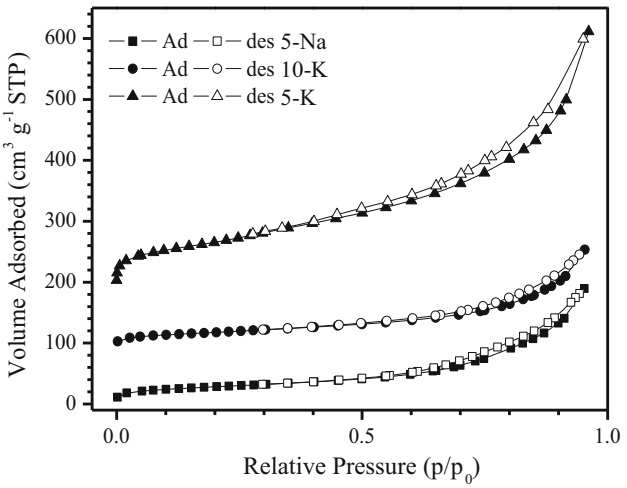

Fig. 4 N_2 adsorption–desorption isotherm for the three sodium and potassium derived alkali-containing samples

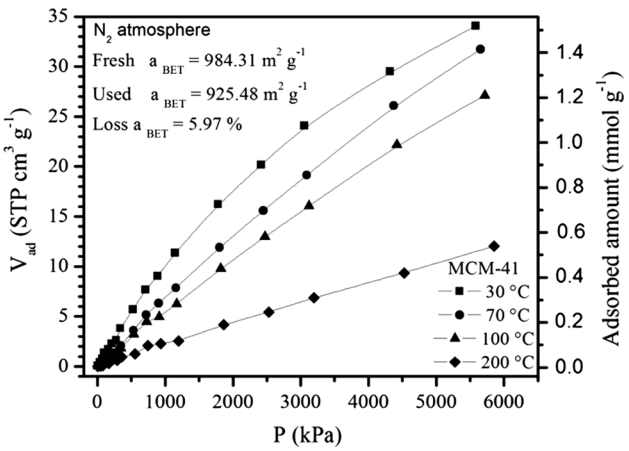

Fig. 6 High pressure N_2 adsorption isotherms at different temperatures for MCM-41

Table 1 Pore structure parameters of mesoporous MCM-41 and derived alkali-containing molecular sieves calculated from N_2 adsorption–desorption

Sample	BET surface área (m^2/g)	Total pore volume (cm^3/g)	Pore diameter ϕ_{pore} (nm)
MCM-41	984.3	1.08	4.3
5Na	100	0.29	11.7
5 K	296.9	0.66	8.8
10 K	92.7	0.25	10.7
Pore structure parameters of impregnated samples after CO_2 sorption			
5Na-100 °C	87.9	0.38	14.5
5 K-100 °C	202.7	0.65	12.9
5 K-200 °C	533.4	1.82	13.6
10 K-100 °C	59.5	0.26	17.7

(0.54 mmol/g) at 5850 kPa. Of course, these changes are in good agreement with the equilibrium temperature–pressure adsorption–desorption processes [24, 25]. To verify the structural and microstructural stability of the sample, the isothermal products were re-characterized. In this case, the structure did not present any change, but the microstructure did show some variations. Specifically, after the high-pressure experiments performed between 30 and 200 °C, the MCM-41 sample presented a surface area decrease of ~6 % (925.4 m^2/g). It may be due to some kind of compaction by effect of the temperature and pressure conditions, the textural characteristics were essentially maintained (pore volume of 0.96 cm^3/g and ϕ_{pore} of 4.11 nm) but it is possible to observe a minimum decrease in the pore diameter size.

Similar to the N_2 adsorption experiments, MCM-41 was tested under similar conditions, switching the flux to CO_2 (Fig. 7). As in the previous case, the CO_2 adsorption decreased as a function of temperature, but the quantities of adsorbed CO_2 were one order of magnitude higher than the adsorbed N_2 amounts. At 30 °C the final quantity of CO_2 adsorbed was 200.02 cm^3/g (8.92 mmol/g). Once the temperature was increased to 70 and 100, the CO_2 adsorption was systematically and significantly decreased to 135.25 and 97.73 cm^3/g (6.03 and 4.36 mmol/g), respectively. However, at 200 and 300 °C the curves exhibit a change in their slopes. The quantity of CO_2 captured decrease significantly at 200 °C were the sample adsorbed 29.18 cm^3/g (1.30 mmol/g) while at 300 °C the maximum amount of CO_2 adsorbed was 0.94 cm^3/g (0.50 mmol/g) at ~2200 kPa. When the pressure was higher than 2000 kPa it was observed a decrease in the CO_2 amount captured because the material was saturated. All these results obtained for the adsorption of N_2 and CO_2 are in good agreement with previously published results on the high pressure gas adsorption tendencies of mesoporous materials such as MCM-41, SBA-15, activated carbons and metal organic frameworks [1, 8–11, 24–29]. Some of the previously obtained results are illustrated schematically in Fig. 7 for comparison purposes.

After the CO_2 sorption studies of the pure MCM-41 sample, the derived alkali-containing samples were tested at two specific temperatures: 100 and 200 °C. Figure 8a shows the CO_2 sorption curves for 5Na, 5 and 10 K at 100 °C. Independently of the alkaline element, the CO_2 adsorbed was higher than the gas captured by the pure sample, despite the fact that all impregnated samples possess smaller surface areas. Once the impregnated samples were analyzed, the final CO_2 adsorptions of 5Na, 5 K and 10 K were 1747.9, 144.57 and 108.04 cm^3/g (77.98, 6.45 and 4.8 mmol/g), respectively. The maximum quantities of adsorbed CO_2 for these samples at ~4200 kPa is very high, if they are compared to other reported values obtained at lower pressures. The CO_2 adsorbed is comparable to other papers related to molecular sieves such as amino-functionalized MCM-41 (9 mmol/g at 3000 kPa and 30 °C [29]) and SBA 15(Cs) (1.4 mmol/g at 100 kPa and

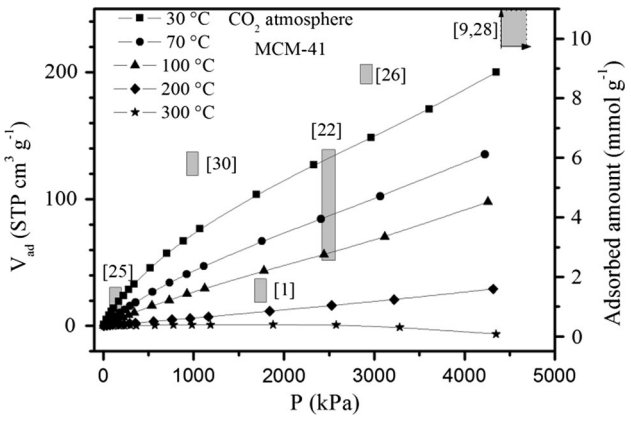

Fig. 7 High pressure CO_2 adsorption isotherms at different temperatures for MCM-41. The *different rectangles* correspond to previous reported data

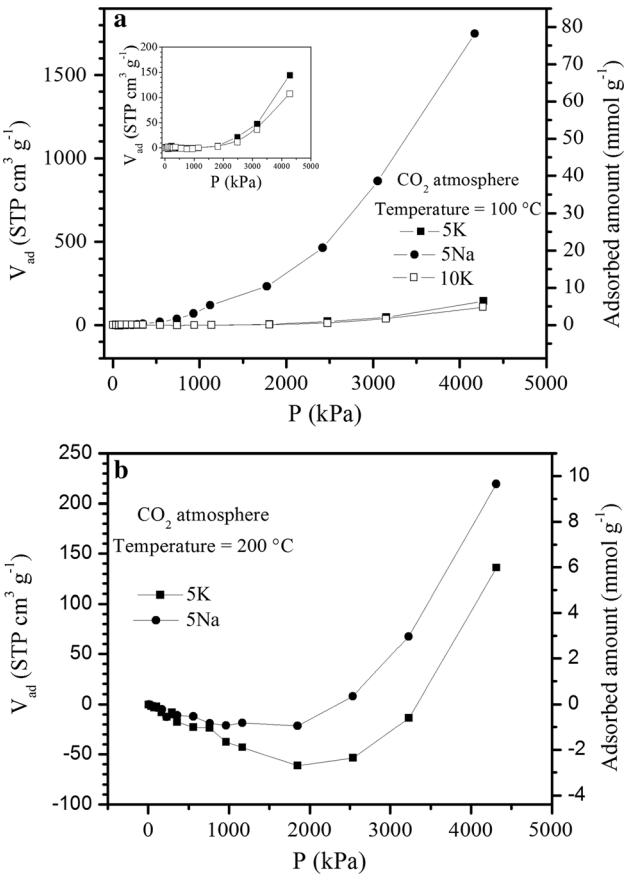

Fig. 8 High pressure CO_2 adsorption isotherms at different temperatures for Na- and K- (5 wt%) derived containing samples, at different temperatures; **a** 100 **b** 200 °C

30 °C [28]) Also, other kind of porous materials have been tested such as MIL-101(Cr) (40 mmol/g at 3500 kPa and 30 °C [30]), MOF-5 (21 mmol/g at 3000 kPa and 30 °C [25], and 20 mmol/g at 5000 kPa and 70 °C [31]), MOF-177 (32 mmol/g at 2500 kPa and 30 °C [25]), zeolites (1.3 mmol/g at 1000 kPa and 30 °C [32]), Na, Cs-RHO zeolite (6 mmol/g at 1000 kPa and 20 °C [33]) and mesoporous CaO (3 mmol/g at 101 kPa and 450 °C [34]) In addition, it should be considered that the synthesis of MCM-41 is simpler and less costly than any MOF-like material, which is an important advantage.

The 5Na sample adsorbed more CO_2 than 5 K, regardless the smaller surface area of 5Na. Therefore, the higher CO_2 adsorption obtained for 5Na may be associated with the larger pore diameter observed in the sample (Table 1). This behavior was confirmed with the experiment performed with the 10 K sample. Although the difference between the pore diameter of the Na and K containing samples is less than 9 % (see Table 1) the CO_2 capture in the 10 K is about 6 % of the total amount adsorbed by the Na containing sample. Although the 5 K sample has the smallest pore diameter, that material captures more CO_2 than 10 K because that sample has the biggest total pore volume, so it is the second important factor in the gases capture at high pressures. This behavior was confirmed with the experiment performed at 200 °C, the CO_2 adsorption behavior was similar (Fig. 8b) although the total amount was less. At this temperature, the 5 wt% Na-containing sample adsorbed more CO_2 than the 5 K sample (9.79 and 6.06 mmol/g, respectively), in the 10 K sample the CO_2 capture amount was irrelevant. At this temperature the adsorption equilibrium shifts to the CO_2 desorption process and hence the total adsorbed volume decreased.

During the CO_2 adsorption the effect of both, the alkaline elements addition and the pressurized CO_2 atmosphere promote the wear of the pore, this was deduct because of the changes in the textural properties shown in Table 1. The change in the pore diameter is 24 % in the 5Na sample, while samples containing K changed between 45 and 65 %. Therefore, under these specific conditions, the CO_2-alkaline element affinities seem to be as important as the microstructural characteristics of the material. To prove this statement the isosteric adsorption heats (Qst) were calculated for the samples with and without alkaline elements.

Figure 9 shows the isosteric heats of adsorption for the pristine MCM-41 and derived alkali-containing samples. The isosteric heats of adsorption are a measurement about the heterogeneity of the material surface; reflecting the interactions between the adsorbent material and the adsorbate (CO_2). Figure 9 shows the interaction between the CO_2 and MCM-41, 5Na, 5 K and 10 K samples. The isosteric heats were calculated from adsorption isotherms at different temperatures in atmospheres of CO_2 and N_2. Initially, the

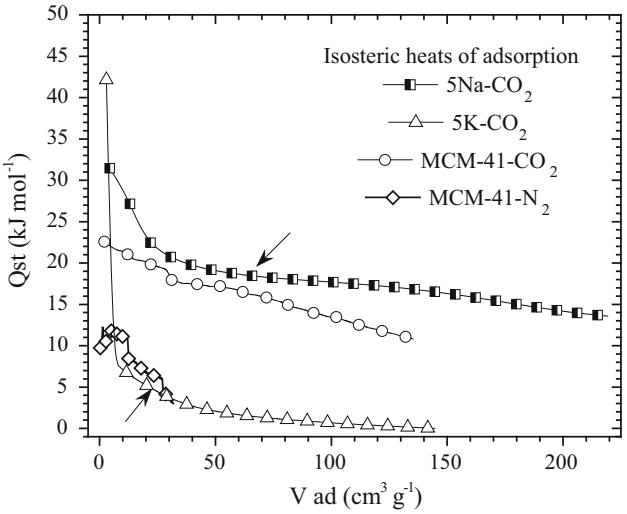

Fig. 9 Isosteric heats of adsorption calculated for pure MCM-41 and derived alkali-containing samples. The *arrows* indicate Vm

isosteric heats measured to the MCM-41 in N_2-atmosphere increase because the first adsorption occurs in the more active sites but the tendency changes abruptly. Despite the pressure reached with N_2, its amount adsorbed was less that the monolayer volume for MCM-41 (226.15 cm/g). In fact, the isosteric heats, for N_2, were the lowest values showing the non-affinity between the gas and the material. Commonly, this kind of materials only physisorb CO_2, as it is possible to observe in the pure MCM-41, the initial Qst was around 20 kJ/mol, which is a typical value for MCM-41 as CO_2 adsorbent. The first Qst values are attributed to CO_2 adsorbed on the active sites (sites of greater affinity) and indeed once these sites are occupied, the Qst decreases. The following values may be attributed to the affinity between the CO_2 molecules and their adsorbed neighbors.

In addition, the 5 K calculated Qst values were the highest at the beginning, but once the adsorption develops, the CO_2 adsorbed amount diminishes. This may be due to the structural evolution of the material. The effect of the pressure and temperature is stronger than the affinity between the material and CO_2. The change in the material was proved because of the textural properties and the XRD pattern changes (see Table 1; Fig. 10). In the case of the samples with Na, the Qst calculated were the highest despite the material structural evolution, showing that the derived alkali-containing sample with Na has the highest affinity to CO_2. The active sites are occupied reaching the monolayer volume (Vm = 22.973 cm^3/g) (>Qst). Then, Qst is stable because the adsorption of the gas is due to CO_2 molecules neighbors.

After the high-pressure experiments performed on the Na- and K-derived alkali-containing samples, the samples were re-characterized using XRD (Fig. 10). Although the samples continued presenting amorphous patterns, some

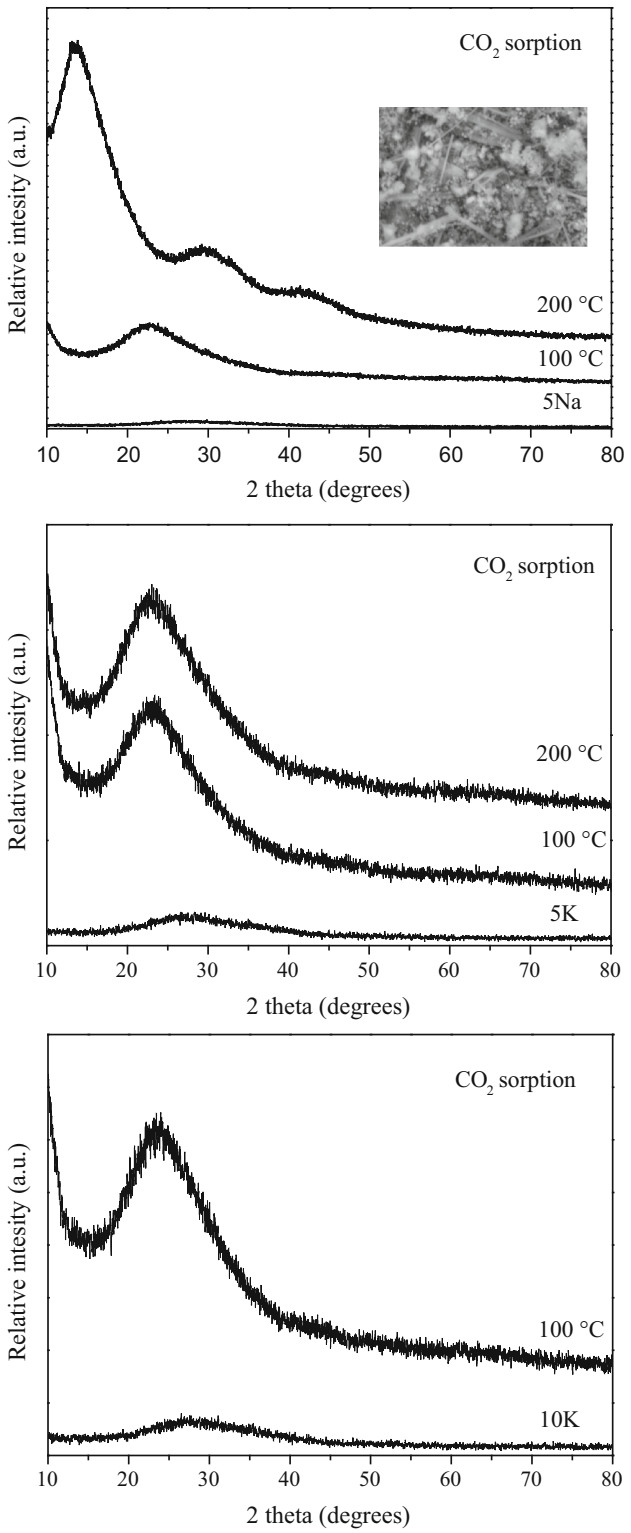

Fig. 10 Standard XRD patterns of 5Na, 5 K and 10 K samples after the CO_2 high pressure adsorptions

defined peaks were observed as a function of the temperature in comparison to the original impregnated samples (Fig. 3). For example, the Na-containing sample developed three wide diffraction peaks centered at 13.7°, 29.4° and 41.7° in the 2θ range. These results strongly suggest a partial structural evolution, where the initial amorphous phase changes to Al–Si–M–O (M = K or Na) crystalline structures. These changes must be produced by the temperature and pressure conditions employed during the CO_2 adsorption experiments. Additionally, at the textural properties and XRD patterns changes, some filament structures were observed in the samples after CO_2 adsorption (see inset in Fig. 10) supporting the fact that a structural evolution of the materials occurred.

4 Conclusions

In this paper, the N_2 and CO_2 adsorption isotherms of MCM-41 molecular sieves and the corresponding Na- and K-derived alkali-containing samples were analyzed at high pressures (4500 kPa) and varying temperatures (30–300 °C). The structure and microstructures of MCM-41 and derived alkali-containing samples were investigated using XRD, IR, and N_2 adsorption. The maximum CO_2 adsorptions of the Na- and K-derived alkali-containing samples at 4000 kPa and 100 °C were 77.98 and 6.45 mmol g^{-1}, respectively. At 200 °C, the CO_2 adsorption trend was similar; nevertheless the CO_2 amount was lower in all cases. The Na-containing sample adsorbed 9.79 mmol/g, and the K-containing sample adsorbed 6.06 mmol/g. The CO_2 capture determined for the pure MCM-41 sample agrees with several previous studies performed at similar pressures and temperatures. However, in this paper, it was analyzed the influence of the incorporation of alkaline cations. The cation addition results in the collapse or destruction of the mesoporous ordering. The alkaline chemical attack seemed to dissolve or destroy two or three pore neighbors, producing a new pore with a larger diameter, resulting in a larger overall pore diameter than that observed in the pure MCM-41.

The addition of an alkaline element positively modified the CO_2 adsorption properties of the mesoporous materials at high pressures as was observed because Qst values. The XRD patterns present a slight variation; suggesting that a structural change occurs during the experiment influenced by pressure, temperature and CO_2 atmosphere. The results showed that the CO_2-alkaline element affinities (surface basicity character) and pore diameter are more important than the surface area, as the impregnated samples shown the highest CO_2 adsorption. Therefore, alkaline addition is a simple and inexpensive method to enhance the CO_2 capture of molecular sieves.

Acknowledgments This work was financially supported by the project SENER-CONACYT and M. J. Ramírez-Moreno thanks to CONACYT for financial support.

References

1. H.M. Yoo, S.Y. Lee, S.J. Park, J. Solid State Chem. **197**, 361 (2013)
2. A. Sayari, Y. Belmabkhout, R. Serna-Guerrero, Chem. Eng. J. **171**, 760 (2011)
3. Y. Belmabkhout, R. Serna-Buerrero, A. Sayari, Chem. Eng. Sci. **64**, 3721 (2009)
4. Y. Belmabkhout, A. Sayari, Chem. Eng. Sci. **64**, 3729 (2009)
5. P. Behrens, G.D. Stucky, Angew. Chem. **105**, 729 (1993)
6. N. Bai, Y. Chi, Y. Zou, W. Pang, Mat. Lett. **54**, 37 (2002)
7. A.S. Araujo, J.M.F.B. Aquino, M.J.B. Souza, A.O.S. Silva, J. Solid State Chem. **171**, 371 (2003)
8. C.C. Costa, D. Ma, A. Melo, M.A.F. Melo, M.E. Mendoza, J.C. Nascimento, J.M. Andrade, J.M.F. Barros, J. Porous Mater. **21**, 1069 (2014)
9. Y. Belmabkhout, G. De Weireld, M. Frère, J. Chem. Eng. Data **49**, 1379 (2004)
10. N. Hedin, L.J. Chen, A. Laaksonen, Nanoscale **2**, 1819 (2010)
11. J. Wu, X. Liu, S.H. Tolbert, J. Phys. Chem. B **104**, 11837 (2000)
12. B. Ma, L. Zhuang, S. Chen, J. Porous Mater. (2015). doi:10.1007/s10934-015-0106-7
13. S.C. Tian, J.G. Jiang, K.M. Li, F. Yang, X.J. Chen, RSC Adv. **4**, 6858 (2014)
14. Q. Wang, Y. Gao, J. Luo, Z. Zhong, A. Borgna, Z. Guo, D. O'Hare, RSC Adv. **3**, 3414 (2013)
15. Z. Luan, H. He, W. Zhou, C.F. Cheng, J. Klinowski, J. Chem. Soc. Faraday Trans. **91**, 2955 (1995)
16. D.D. Dharani, P.J.E. Harlick, A. Sayari, Catal. Comm. **8**, 829 (2007)
17. S.C.G. Santos, S.W.M. Machado, A.M. Garrido-Pedrosa, M.J.B. Souza, J. Porous Mater. **22**, 1145 (2015)
18. S. Cavenati, C.A. Grande, A.E. Rodriguez, J. Chem Data **49**, 1095 (2004)
19. S.C. Zhuo, Y.M. Huang, J. Hu, H.L. Liu, Y. Hu, J.W. Jiang, J. Phys. Chem. C **112**, 11295 (2008)
20. S. Lowell, J.E. Shields, M.A. Thomas, *Characterization of Porous Solids and Powders: Surface, Area, Pore Size and Density* (Kluwer Academic Publishers, Springer, London, 2004), pp. 58–80
21. E.M. McCash, *Surface Chemistry* (Oxford University Press, Oxford, 2002)
22. J. Rouquerol, F. Rouquerol, P. Llewellyn, G. Maurin, K.S.W. Sing, *Adsorption by Powders and Porous Solids. Principles, Methodology and Applications*, 2nd edn. (Academic Press, Elsevier, Oxford University Press, Oxford, 2014), pp. 1–58
23. J.B. Condon, *Surface Area and Porosity Determinations by Physisorption, Measurements and Theory* (Elsevier, Oxford University Press, Oxford, 2006), pp. 1–28
24. J.C. Fisher, R.V. Siriwardane, R.W. Stevens, Ind. Eng. Chem. Res. **50**, 13962 (2011)
25. R.V. Siriwardane, M.S. Shen, E.P. Fisher, Energy Fuels **15**, 279 (2001)
26. S. Loganathan, M. Tikmani, A.K. Ghoshal, Langmuir **29**, 3491 (2013)
27. A.R. Millward, O.M. Yaghi, J. Am. Chem. Soc. **127**, 17998 (2005)
28. A. Zukal, J. Mayerova, J. Cejka, Phys. Chem. Chem. Phys. **12**, 5240 (2010)
29. T. Custódio dos Santos, S. Bourrelly, P.L. Llewellyn, J. de Walkimar, M.C. Machado Ronconi, Phys. Chem. Chem. Phys. **17**, 11095 (2015)
30. P.L. Llewellyn, S. Bourrelly, C. Serre, A. Vimont, M. Daturi, L. Hamon, G. De Weireld, J. Chang, D. Hong, Y.K. Hwang, S.H. Jhung, G. Ferey, Langmuir **24**, 7245 (2008)
31. J.Y. Jung, F. Karadas, S. Zulfiqar, E. Deniz, S. Aparicio, M. Atilhan, C.T. Yavuz, S.M. Han, Phys. Chem. Chem. Phys. **15**, 14319 (2013)
32. J. Perez-Carbajo, P. Gómez-Álvarez, R. Bueno-Perez, P.J. Merkling, S. Calero, Phys. Chem. Chem. Phys. **16**, 5678 (2014)
33. M. Pera-Titus, M. Palomino, S. Valencia, F. Rey, Phys. Chem. Chem. Phys. **16**, 24391 (2014)
34. Z. Wu, N. Hao, G. Xiao, L. Liu, P. Webley, D. Zhao, Phys. Chem. Chem. Phys. **13**, 2495 (2011)